Reliability Assessment of Interconnected Power Systems with HVDC Links Considering Frequency Regulation Process

Chengjin Ye, Libang Guo, Yi Ding, Ming Ding, Peng Wang, and Lei Wang

***Abstract*—With various components and complex topologies, the applications of high-voltage direct current (HVDC) links bring new challenges to the interconnected power systems in the aspect of frequency security, which further influence their reliability performances. Consequently, this paper presents an approach to evaluate the impacts of the HVDC link outage on the reliability of interconnected power system considering the frequency regulation process during system contingencies. Firstly, a multi-state model of an HVDC link with different available loading rates (ALRs) is established based on its reliability network. Then, dynamic frequency response models of the interconnected power system are presented and integrated with a novel frequency regulation scheme enabled by the HVDC link. The proposed scheme exploits the temporary overload capability of normal converters to compensate for the imbalanced power during system contingencies. Moreover, it offers frequency support that enables the frequency regulation reserves of the sending-end and receiving-end power systems to be mutually available. Several indices are established to measure the system reliability based on the given models in terms of abnormal frequency duration, frequency deviation, and energy losses of the frequency regulation process during system contingencies. Finally, a modified two-area reliability test system (RTS) with an HVDC link is adopted to verify the proposed approach.**

***Index Terms*—Reliability, multi-state modeling, interconnected power system, high-voltage direct current (HVDC) link, frequency regulation.**

NOMENCLATURE

λ_s, μ_s	Failure and repair rates of series subsystem
λ_i, μ_i	Failure and repair rates of component i
λ_{CS}, μ_{CS}	Failure and repair rates of a converter system (CS)
λ_{TS}, μ_{TS}	Failure and repair rates of a transmission system (TS)
λ_{FS}, μ_{FS}	Failure and repair rates of a filter system (FS)
λ_g, μ_g	Failure and repair rates of a generator
A_g, U_g	Availability and unavailability of a generator
$A_{g,i}$, $U_{g,i}$	Availability and unavailability of normal and failed generators in generation system
c_k	Available loading rate (ALR) state of high-voltage direct current (HVDC) link
C	Set of potential ALRs
D	Load damping rate
F_{HP}	Equivalent high-pressure power fraction of reheat turbine
f^L	Frequency limit
$\Delta f_{S,t}$	Frequency deviation of sending-end (SE) AC power system
$\Delta f_{R,t}$	Frequency deviation of receiving-end (RE) AC power system
H_g, S_g	Inertia and rated apparent power of generator g
IS_S, IS_R	Security indicators of SE and RE AC power systems
K_{AGC}	Auto generation control (AGC) system gain
$K_{AGC,i}$	AGC system gain of generation i
LSR_s	Energy loss in RE AC power systems with system contingency s
LSR_t	Measured energy curtailment in time t
M, N	Sets of outage combinations (OCs) included in ALR states X and Y
N_G	Sets of all generators
$N_{G,F}$	Sets of all failed generators
$N_{G,C}$	Sets of committed generators
$\boldsymbol{P}$	Vector of state probability
p_i	Probability of OC i obtained from $\boldsymbol{P}$
PR_t^G	Power reserve value during period t in RE AC power system
ΔPR_t	Power imbalance value during period t in RE AC power system

Manuscript received: July 19, 2021; revised: October 8, 2021; accepted: December 15, 2021. Date of CrossCheck: December 15, 2021. Date of online publication: January 14, 2022.

This work was supported by the National Science Foundation of China (No. 51807173), the Foundation Research Funds for Central Universities (No. 2021QNA4012), and the Project of State Grid Zhejiang Electric Power Co., Ltd. (No. 2021ZK11).

C. Ye, L. Guo (corresponding author), and Y. Ding are with the College of Electrical Engineering, Zhejiang University, Hangzhou, China (e-mail: yechenjing@zju.edu.cn; jamesguo95@zju.edu.cn; yiding@zju.edu.cn).

M. Ding is with the School of Electrical Engineering and Automation, Hefei University of Technology, Hefei, China (e-mail: mingding56@126.com).

P. Wang is with the Electrical and Electronic Engineering School, Nanyang Technological University, Singapore (e-mail: epwang@ntu.edu.sg).

L. Wang is with the State Grid Zhejiang Electric Power Co., Economic and Technological Research Institute, Hangzhou, China (e-mail: wang_lei1@zj.sgcc.com.cn).

DOI: 10.35833/MPCE.2021.000491

P_t^R	Reduced transmission power
P_t^I	Increased transmission power
P_t^N	Rated transmission power of HVDC link
$p_{t,s}$	Probability of system contingency s during period t
p_X	Probability of equivalent ALR state
$q_{i\to j}$	Transition rate from OC i to j
R, T_G	Equivalent governor speed regulation and time constants
R_i, $T_{G,g}$	Governor speed regulation and time constants of generator g
R^L	Limit of rate-of-change-of-frequency (RoCoF)
R_p^D, R_p^U	Downward and upward reserve capacities of primary frequency response (PFR)
r_k	Overload rate of HVDC link
r_v, r_f	Preset control gain parameters
S	Set of potential contingencies
$Sat_P(x)$	Saturation block of PFR
$Sat_{S_1}(x)$	Saturation block denoting ramping capacities of SFR
$Sat_{S_2}(x)$	Saturation block denoting reserve capacities of SFR
T	Whole period of system contingency
T_{CH}, T_{RH}	Equivalent steam chest and reheat turbine time constants
T_P	Required time period to stabilize the system frequency by PFR
TS_s^A, TR_s^A	Durations of frequency abnormal of SE and RE AC power systems
TS_s^P, TS_s^S	Durations of PFR and SFR models of SE AC power system
TR_s^P, TR_s^S	Durations of PFR and SFR models of RE AC power system
$\Delta V_{DC,t}$	DC voltage variation
$\boldsymbol{Z}_{HVDC}$	Stochastic transitional probability matrix of bipolar HVDC link
$\boldsymbol{Z}_{OC}$	Stochastic transitional probability matrix

I. Introduction

HIGH-VOLTAGE direct current (HVDC) transmission technology has become an ideal solution for the bulk power transfer over long distances between the economic generation areas and the large load centers in recent decades [1]. As the HVDC links are superior to the traditional AC links in terms of large capacity and low loss, they are mainly applied in interconnecting several asynchronous AC power systems with independent frequency and phase angles [2]. For now, many HVDC projects have been well operated in China, including the Yunnan-Guangdong ultra-HVDC, the Jinping-Sunan ultra-HVDC, as well as the Xiluodu-Zhejiang ultra-HVDC projects, etc. [3]-[5].

The deployment of HVDC links brings challenges in terms of frequency security to the interconnected power systems. To begin with, the frequent failures of the HVDC link may raise great power imbalances that cause severe frequency deviation. With massive components and complex topologies, it is more likely that failures occur at HVDC links compared with AC links. Besides, since the HVDC link usually contains millions of megawatts of power flow, its failures may cause severe power imbalances for both the sending-end (SE) and receiving-end (RE) AC power systems. Such severe power imbalances caused by the outages of HVDC link are much likely to cause terrible frequency deviation in either side of the interconnected power system. For instance, the bi-polar block accident in the Jinping-Sunan ultra-HVDC caused a power loss of over 4000 MW and then led to a frequency drop of 0.44 Hz in the Eastern China grid on September 19, 2015 [6]. Moreover, the low-inertia characteristics of HVDC link make the frequency deviation difficult to be automatically eliminated in time by the interconnected system. Unlike the conventional AC link which can be inherently responsive to the changes of system frequency, the HVDC link connects asynchronous AC power systems through the non-synchronous interfaces, and thus shows low-inertia characteristics to the frequency variation [7]. Such a low-inertia feature may cut down the frequency regulation capability of interconnected power systems. Therefore, when a disturbance in the system frequency occurs due to the great power imbalances caused by the HVDC link outages, the existing frequency regulation capability may be insufficient to stabilize the system frequency, which increases the abnormal frequency duration. Still taking the aforementioned bipolar block accident in the Jinping-Sunan ultra-HVDC as an example, the reduced frequency regulation capability rendered the frequency deviation duration to last for over 200 s [6]. Overall, the frequency deviation and abnormal duration caused by power imbalances will significantly affect the reliable operation of interconnected power systems. Therefore, it is imperative for operators to evaluate the reliability of interconnected power systems with HVDC links in terms of the frequency dynamics during its regulation process initiated by the great power imbalances due to the HVDC link failures.

Considering the significant impacts of the HVDC link faults, several studies have been conducted on reliability modeling. Some of them focus on component-level analysis. In [8], a reliability model of modular multi-level converter in the voltage-source-based HVDC link considering periodic preventive maintenance is proposed. The reliability of the converter transformers (CTs) in an ultra-HVDC link is quantified in [9] by the state space and frequency & duration approaches. Besides, there are also many works aiming at evaluating the system-level reliability of the HVDC link. In [10], a reliability evaluation model and a bi-level unreliability allocation model for the ±500 kV HVDC link with the double-circuit lines on the same tower are given, in which the reliability evaluation indices associated with the DCLST HVDC link is defined. A reliability equivalent approach for an HVDC link considering the CT winding, the states with half capacity, and the passive reserve shutdown is derived in [11]. In [12], a novel ultra-HVDC reliability model and an evaluation approach are proposed, which successfully reduces the dimension of the complex state space solution. How-

ever, the above previous reliability modeling studies have not taken the frequency dynamics of the interconnected power systems during contingencies into account. As mentioned above, with the application of HVDC links, the significant frequency deviation following the great power imbalances due to the HVDC link failures will also bring risks for the reliability of the interconnected power system. Consequently, the corresponding frequency regulation process for frequency deviation should also be considered in the reliability evaluation.

Meanwhile, due to the low-inertia feature, it has become a real concern how the abnormal frequency duration of interconnected power systems caused by the HVDC link failures can be effectively reduced. Some works have focused on regulating frequency with spinning reserves. In [13], a cost-efficient contingency reserve allocation scheme for the combined HVDC and RE AC power system is studied. The virtual inertia provided by energy storage systems in HVDC interconnected systems is discussed in [14]. Others have made efforts in investigating new HVDC control schemes to give active frequency support based on the fast regulation capability of the HVDC links. In [15], the frequency stability of the SE AC power system is studied in terms of the given control schemes. An HVDC control scheme with local measurements and actions to provide frequency support is proposed in [16]. Nevertheless, the models used in above studies for regulating the frequency deviation in the interconnected power system cannot reflect the detailed energy curtailment involved in the frequency regulation process by their performance standards, which are important for analyzing reliability performance during the frequency regulation process. Since this paper focuses on the reliability analysis, these models should be modified for reliability evaluation to provide detailed energy information for the reserve, and frequency regulation management of power system operation.

Furthermore, the conventional approaches for reliability assessment utilize reliability indices such as the expected energy not supplied (EENS) and the loss of load probability (LOLP), which do not depict the frequency-related reliability such as the frequency deviation and the abnormal frequency duration. Although [17] has proposed some indices for reliability evaluation considering the frequency regulation process, the frequency dynamics are simplified as a linear relationship in this paper, and the key frequency variation features, such as the frequency slope and the duration of abnormal frequency, still cannot be well characterized. In general, the current techniques and indices cannot effectively assess the impact of the HVDC link outages and associated frequency regulation process on the reliability performance of the interconnected power systems.

Given this background, this paper proposes an approach for system operators to evaluate the reliability performance of interconnected power systems with HVDC links considering the frequency regulation process during system contingencies. Firstly, a multi-state model of an HVDC link is developed with different available loading rates (ALRs) and the corresponding probabilities. Then, the models for the primary frequency response (PFR) and secondary frequency response (SFR) of the interconnected power systems are integrated with a support scheme provided by the HVDC link for system frequency regulation. In this scheme, the converters under normal operation will temporarily carry out overload transmission to mitigate the power imbalance that causes frequency disturbance for both SE and RE AC power systems under system contingencies. Meanwhile, the proposed scheme can transmit the frequency deviation at the fault end to the opposite end through the DC voltage variation. The opposite end then feeds such deviation signal into its frequency regulation framework to dispatch reserves against the power vacancy. In this way, the mutual energy aid between reserves of both sides can be characterized, and the energy losses during the frequency regulation process can be detected for reliability analysis. Finally, several reliability indices are proposed to represent the frequency dynamics and energy losses during the frequency regulation process, which is evaluated by the Monte Carlo simulation (MCS) technique.

II. Multi-state Model of HVDC Link

In this section, the multi-state model of an HVDC link is proposed. The multi-state model can effectively reflect different performance levels and the corresponding probabilities of composite systems in a simplified expression, and has been used in many reliability analyses [18]. The studied HVDC link is bipolar with two 12-pulse converters connected with both SE and RE AC power systems. The main components in the HVDC link include AC filter (ACF), breaker (Brk), CT, converter valve (CV), converter protection and control (PC) system, DC filter (DCF), and DC transmission line (DCL) [12]. The reliability network of the HVDC link considering these main components are illustrated in Fig. 1. It should be noted that the actual system and the reliability network used to model the system may not necessarily have the same topological structure [19], [20].

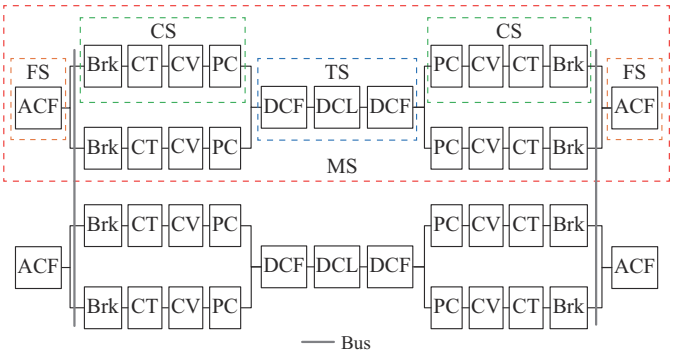

Fig. 1. Reliability network of a bipolar HVDC link.

Based on the impact of different component failures on the ALRs, the reliability network of an HVDC link can be divided into three kinds of subsystems, namely filter system (FS), converter system (CS), and transmission system (TS). These three kinds of subsystems combine a monopole system (MS) of an HVDC link. Except for an FS that is composed of an ACF, each CS or TS can be regarded as an equivalent series element with several components, as shown

in Fig. 1. The equivalent failure and repair rates of a series subsystem can be calculated as [20]:

$$\lambda_s = \sum_i \lambda_i \tag{1}$$

$$\mu_s = \sum_i \lambda_i \mu_i \Big/ \sum_i \lambda_i \tag{2}$$

In this paper, the lifespan of the main component in the HVDC link is assumed to be exponentially distributed, and these components work during the "constant failure rate period" [11], [12], which means that λ_i and μ_i are considered to be constant. Therefore, through (1) and (2), the equivalent failure and repair rates of a CS (λ_{CS}, μ_{CS}) and a TS (λ_{TS}, μ_{TS}) can be obtained, while the failure and repair rate of an FS (λ_{FS}, μ_{FS}) is equal to that of an ACF.

After series equivalence, an MS can be modeled as an equivalent series-parallel element as shown in the red dash rectangle of Fig. 1. In the equivalent series-parallel element of MS, two CSs are linked in parallel and then combined with other two CSs linked in parallel, two FSs, and one TS in series. Besides, with two MSs linked in parallel, an HVDC link can be regarded as a multi-state model with different performance levels in terms of ALRs.

In the following subsections, the state space diagram for an MS of a bipolar HVDC link is firstly developed. Then, two separate state space diagrams of MS are aggregated to build the multi-state model of a bipolar HVDC link.

A. State Space Diagram for an MS of a Bipolar HVDC Link

As shown in Fig. 1, each MS of the HVDC link consists of four CSs, two FSs, and one TS. Meanwhile, since the CSs and FSs are symmetrically linked, the fault of any FS or the outage of any CS in the CSs linked in parallel will have the same influence. Considering this symmetry feature, there are eleven outage combinations (OCs) in the state space diagram of an MS, as shown in Fig. 2, where the upper left number of each block represents the OC number. The shaded subsystems in Fig. 2 represent the failed ones. It should be noted that when the MS totally breaks down (e.g., OC4-11 in Fig. 2), the subsystems in the MS are considered to be out of operation. Under such a circumstance, no further subsystem outage will occur while the fault subsystems can still be repaired [12].

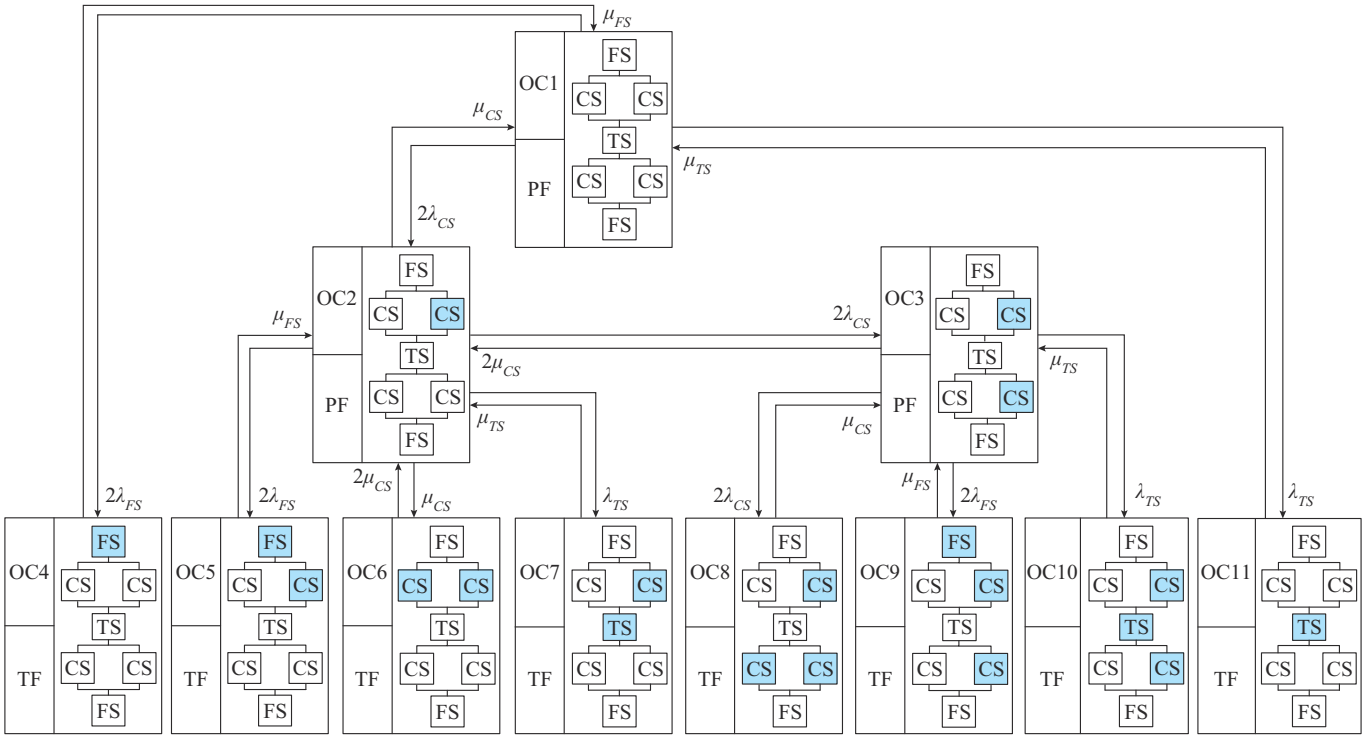

Fig. 2. State space diagram of an MS.

Meanwhile, based on the usage of the state space diagram defined in [19], the state space diagram translates the operation state of an MS in Fig. 1 into a mathematical model that can be solved by using the Markov process. Hence, based on the state space diagram given in Fig. 2, the probability of each OC can be calculated by solving the differential equations describing the Markov process [19]:

$$\begin{cases} \partial \boldsymbol{P}/\partial t = \boldsymbol{Z}_{OC}\boldsymbol{P} \\ \boldsymbol{P} = [p_{OC1}, p_{OC2}, \ldots, p_{OC11}] \end{cases} \tag{3}$$

The row position of $\boldsymbol{Z}_{OC}$ is the OC, from which the transition occurs and the column position of $\boldsymbol{Z}_{OC}$ is the OC at which the transition occurs. Since there are 11 OCs for an MS in total, $\boldsymbol{Z}_{OC}$ is a 11×11 matrix whose elements are:

$$\begin{cases} Z_{OC,ij} = q_{i\to j} & i \neq j \\ Z_{OC,ii} = -\sum_{i\neq j} Z_{ij} \end{cases} \tag{4}$$

$q_{i\to j}$ equals to failure or repair rate of the corresponding subsystem according to the changes between the two OCs

(e.g., λ_{CS}, μ_{CS}, λ_{TS}, μ_{TS}, λ_{FS}, and μ_{FS}).

Besides, different OCs may lead to the same ALR, and the OCs with identical ALR can be merged into an equivalent state. Hence, the OCs of an MS can be aggregated into three equivalent ALR states, including the normal (N) state, the partial failure (PF) state, and the total failure (TF) state, as given in the lower left number of each block in Fig. 2. The aggregated state space diagram of an MS is given in Fig. 3, including both the equivalent ALR states (states 1-3) and the corresponding transition rates between the equivalent ALR states (λ_{NT}, μ_{TN}, λ_{NP}, μ_{PN}, λ_{PT}, and μ_{TP}).

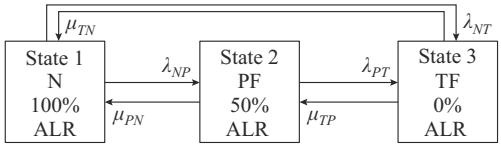

Fig. 3. Aggregated state space diagram of an MS.

Through the state merging technique given in [21], the probabilities of the three equivalent ALR states and the corresponding transition rates can be calculated by:

$$p_X = \sum_{i \in M} p_i \tag{5}$$

$$q_{X \to Y} = \frac{1}{p_X} \sum_{i \in M} p_i \sum_{j \in N} q_{i \to j} \tag{6}$$

Taking the transition from state 1 to state 2 in Fig. 3 as an example, as shown in Fig. 2, OC1 can be regarded as state 1, while the OC2 and OC3 have the same ALR, and can be merged into the state 2. Then, the state probability p_2 and transition rate λ_{NP} can be calculated by:

$$\begin{cases} p_2 = p_{OC2} + p_{OC3} \\ \lambda_{NP} = (p_{OC1} \cdot 4\lambda_{CS}) / (p_{OC2} + p_{OC3}) \end{cases} \tag{7}$$

B. State Space Diagram for a Bipolar HVDC Link

As observed from Fig. 1, a bipolar HVDC link is made up of two MSs linked in parallel. Therefore, the reliability model of a bipolar HVDC link is developed by combining two separate MS state space diagrams in this paper.

Since each MS has three ALR states as given in the last subsection, by combining each state of MS in pairs, a state space diagram of a bipolar HVDC link with nine system states can be obtained, as illustrated in Fig. 4. In the state space diagram, each system state can be specified through a two-element vector indicating the ALR states of the two MSs. For instance, the vector of system state 2 is (PF, N), which means that one MS partially fails and the other one operates normally, respectively.

The probability of system state of the bipolar HVDC link can be calculated by solving the differential equations describing the Markov process in the same form as (3) based on the stochastic transitional probability matrix of the bipolar HVDC link $\boldsymbol{Z}_{HVDC}$ built by the state transition rates, e.g., λ_{NP}, μ_{PN} in Fig. 4. Besides, similar to the state space diagram of an MS, different system states of a bipolar HVDC link can also have the same loading performance. Therefore, assuming that each MS shares its loading equally, and that the two CSs linked in parallel also have the same loading rates, by using the state merging technique given in [22], the nine system states of a bipolar HVDC link can be aggregated into five equivalent states with different ALRs, as given in Table I. The probabilities of the equivalent ALR states of the bipolar HVDC link can also be obtained by adding the probabilities of system states in Fig. 4 with the same ALRs.

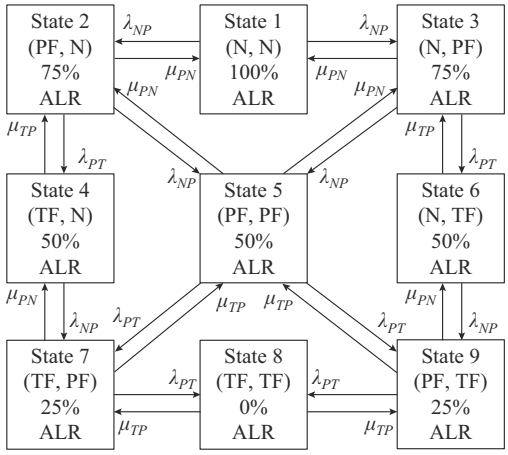

Fig. 4. State space diagram for a bipolar VSC-HVDC link.

TABLE I
EQUIVALENT ALR STATES OF A BIPOLAR HVDC LINK

State	Explanation
100% ALR	The system is in normal state with no MS failures
75% ALR	Partial failure occurs in one MS while the other MS is normal, causing a 25% derating of loading
50% ALR	One MS totally fails while the other MS is normal, or both MSs partially fail
25% ALR	Partial failure occurs in one MS, while the other MS is in total failure state
0% ALR	It is the worst operation state as both MSs totally fail

III. MULTI-STATE MODEL OF GENERATION SYSTEMS

In addition to the failure of the HVDC link, the outages of generators may also result in the loss of power supply and cause power imbalance. In this section, the multi-state model to characterize the reduction of power supply and the corresponding probabilities of generation system in either side of the interconnected power system is proposed.

Typically, the reliability performance of generators is evaluated by a two-state model with constant failure and repair rate [17]. The availability A_g and unavailability U_g of generator g are obtained by:

$$A_g = \mu_g / (\lambda_g + \mu_g) \tag{8}$$

$$U_g = \lambda_g / (\lambda_g + \mu_g) \tag{9}$$

Meanwhile, the generation systems in the SE or RE AC power systems are usually made up of multiple generators. The outage of each generator will cause a reduction in the output of the whole generation system. For a generation system with N_G generators, assuming that a reduction of PR^G in the output is caused by $N_{G,F}$ failed generators, the corresponding probability p_R for the reduced output is:

$$p_R = \prod_{i=1}^{N_{G,F}} U_{g,i} \prod_{i=N_{G,F}+1}^{N_G} A_{g,i} \tag{10}$$

IV. Frequency Regulation Scheme Provided by HVDC Link

In this section, the frequency regulation scheme provided by the HVDC link is given. Firstly, the conventional frequency regulation scheme with PFR and SFR models is presented. Then, based on the multi-state models of the HVDC link and generation systems, the power imbalance causing frequency disturbance during system contingencies is obtained. Finally, according to the obtained power imbalance as well as the PFR and SFR models, a frequency support scheme provided by the HVDC link is formulated and applied to different contingencies.

A. Conventional Frequency Regulation Scheme

The conventional frequency regulation scheme includes the PFR and SFR models and has been widely adopted to maintain the frequency stability. A block diagram of the conventional frequency regulation scheme is shown in Fig. 5, where x_G, x_{CH}, x_{RH}, x_{FR}, and x_{AGC} are the output variables of generators, equivalent steam chest, reheat turbine, frequent response, and AGC, respectively.

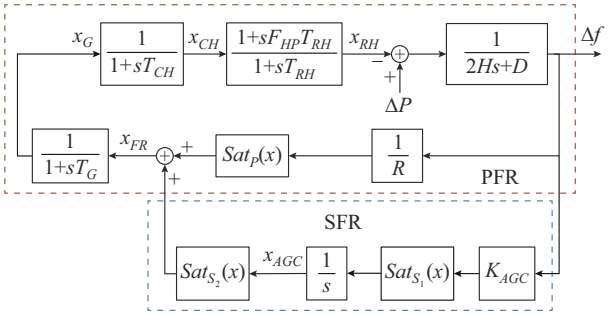

Fig. 5. Block diagram of conventional frequency regulation scheme.

The model of PFR can be represented in the upper part of Fig. 5 [21], [23], [24]. The input and output (ΔP and Δf) are the system power imbalance and the frequency deviation, respectively. H is the equivalent system inertia evaluated by:

$$H = \frac{\sum_{g \in N_{G,C}} H_g S_g}{\sum_{g \in N_{G,C}} S_g} \tag{11}$$

The equivalent governor speed regulation and time constants, R and T_G, can be evaluated by:

$$\frac{1}{R} = \sum_{g \in G_c} \frac{S_g}{R_g} \Big/ \sum_{g \in G_c} S_g \tag{12}$$

$$T_G = \sum_{g \in G_c} T_{G,g} S_g \Big/ \sum_{g \in G_c} S_g \tag{13}$$

where G_c is the set of generators. It can be observed that $1/R$ and T_G are the averages of $1/R_g$ and $T_{G,g}$ weighted by S_g. The equivalent parameters can also be obtained by calculating the corresponding weighted averages of generators. The saturation block of PFR is represented by $Sat_P(x)$, where the input of the block x is restricted between the downward reserve capacity R_p^D and upward reserve capacity R_p^U of PFR.

Meanwhile, SFR is integrated with the PFR, as shown in the lower part of Fig. 5. Since the SFR is activated after the frequency is stabilized, the automatic generation control (AGC) system gain K_{AGC} is constructed as a time-variant parameter and defined as:

$$K_{AGC}(t) = \begin{cases} 0 & t < T_P \\ \sum_{g \in G_c} K_{AGC,g} S_g \Big/ \sum_{g \in G_c} S_g & t > T_P \end{cases} \tag{14}$$

B. Imbalanced Power During Contingencies

During system contingencies, although the failures of HVDC link may lead to severe power imbalance, the temporary overload capability of normal converters in the HVDC link can still be exploited to compensate for the imbalanced power, and thus, regulate the following frequency deviation [25]. In detail, when a contingency occurs, the normal converters in the HVDC link can increase their transmission power by a certain overload rate after exploiting the regular allowance to offset the power losses to some extent. In practice, the overload rate is mainly restricted to the thermal rating of the key equipment of the HVDC link, such as CV, CT, and ACF [26]. It is also subject to the overload duration [25]. Considering the primary frequency regulation process that usually lasts for a few seconds, the transient overload rate is adopted in this paper. Besides, the overload rate is set to be associated with the ALR of the HVDC link during system contingencies with the following parts specifically.

1) When the ALR of the HVDC link is 75% or higher, the transmission power of the normal converters can be increased by overload rate r_{k1}.

2) When the ALR of the HVDC link decreases to 50% or below, the transmission power of the normal converters can be lifted by another overload rate r_{k2}, which is higher than r_{k1}. Hence, the transmission power increment can be as close as possible to the one with higher ALR.

For instance, assuming that an exemplary system contingency contains a partial failure at the HVDC link and failure of $N_{G,F}$ generators in the RE AC power system, the power imbalance that causes the frequency disturbance can be formulated as:

$$\Delta PR_t = PR_t^G + P_t^R - P_t^I \tag{15}$$

P_t^R and P_t^I can be obtained by:

$$\begin{cases} P_t^R = (1 - c_k) P_t^N \\ 0 \le P_t^I \le r_k c_k P_t^N \\ r_k \in \{r_{k1}, r_{k2}\} \\ c_k \in C = \{1, 0.75, 0.5, 0.25, 0\} \end{cases} \tag{16}$$

Based on the multi-state model of the HVDC link, C contains five equivalent ALR states given in Table I.

Since the reliability parameters such as failure rates of AC transmission networks are typically much lower than those of generators, the transmission networks in the SE and RE AC power systems are assumed to be fully reliable in this

paper. Besides, the transmission constraints and power flows of SE and RE AC power systems are also not considered to ensure the overall efficacy of the proposed solution, which should be improved in further studies. To mitigate the transmission congestions during system contingencies, the dynamic transmission rating (DTR) system is a potential solution [27], [28], which can increase the thermal constraint and subsequently maximum loading of existing transmission lines.

C. Proposed Frequency Support Scheme

Based on the frequency response models of PFR and SFR, a frequency support scheme provided by the HVDC link is formulated to eliminate the frequency deviation caused by the power imbalance during system contingencies. Still using the same system contingency as an example, a diagram of the frequency support scheme with the exemplary system contingency is given in Fig. 6.

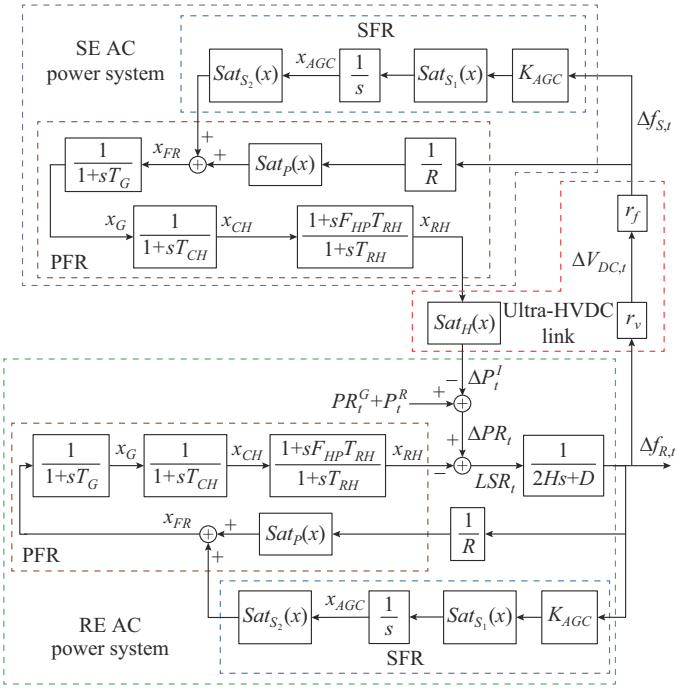

Fig. 6. Diagram of frequency support scheme with exemplary system contingency.

Specifically, when the system contingency occurs, the power imbalance ΔPR_t can be obtained through (15). Then, based on the combined PFR and SFR models of the RE AC power system, the frequency deviation of the RE AC power system $\Delta f_{R,t}$ is measured. Then, a two-step frequency-voltage control of the HVDC link is activated. In detail, the DC voltage of the connected converter between the HVDC link and RE AC power system is adjusted based on $\Delta f_{R,t}$. Furthermore, the DC voltage variation $\Delta V_{DC,t}$ is used to produce an equivalent frequency deviation signal $\Delta f_{S,t}$ to the SE AC power system. The relationship between frequency deviation and voltage variation during the whole control process is given by [16]:

$$\Delta V_{DC,t} = r_v \Delta f_{R,t} \tag{17}$$

$$\Delta f_{S,t} = r_f \Delta V_{DC,t} \tag{18}$$

The frequency deviation signal $\Delta f_{S,t}$ is transmitted to the SE AC power system through communication system. Based on $\Delta f_{S,t}$, the generators in the SE AC power system will put in their reserves to support the RE AC power system, which is achieved by the PFR and SFR mechanisms of the SE system. The increased output ΔPS_t^G will be transmitted to the RE AC power system through the HVDC link and converted into the transmission power increment P_t^I by a saturation block $Sat_H(x)$, which denotes the transmission limit of the HVDC link. The saturation threshold of $Sat_H(x)$ is adjusted subject to the ALR of the HVDC link and the temporary overload rate of normal converters, as given in (16).

As observed from the above scheme, by utilizing the temporary overload capability of normal converters, the power imbalance ΔPR_t can be compensated by P_t^I, and the frequency regulation resources of the RE AC power system will be greatly enhanced. For better demonstration, the schematic frequency dynamics of SE and RE AC power systems subject to the exemplary system contingency with and without the proposed frequency support scheme is shown in Fig. 7.

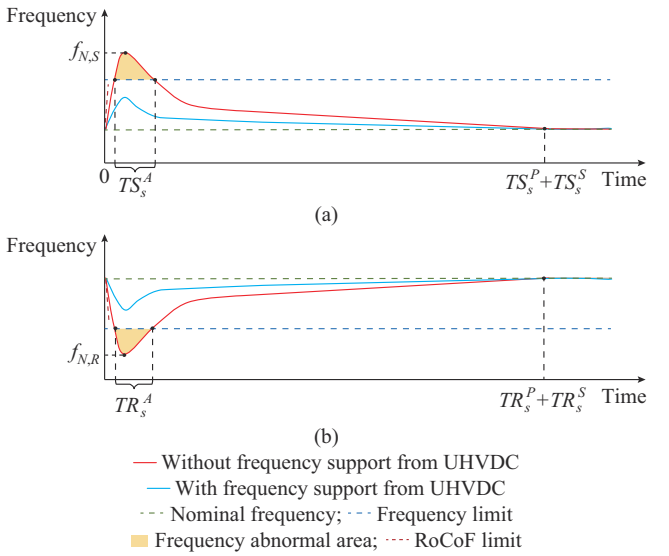

Fig. 7. Schematic frequency dynamics of SE and RE AC power systems. (a) SE AC power system. (b) RE AC power system.

In the SE AC power system, there is an excess of power supply due to the power transmission block caused by the HVDC link outage, which leads to a rising tendency of frequency. On the other hand, the falling tendency of frequency in the RE AC power system is quite obvious due to the shortage of power supply. With the proposed frequency support scheme, the frequency dynamics at both ends are modified. Specifically, the characteristics of frequency profile change in many aspects, including the variation sharp rate, the greatest deviation to the nominal, the duration and the abnormal frequency area. Meanwhile, for the system contingencies where the generator outage occurs in the SE AC power system, the support scheme is similar. In such a case, the generators in the RE AC power system will increase their power outputs, and therefore, the HVDC link can reduce its transmission power to relieve the power imbalance in the SE AC power system.

With the proposed frequency support scheme, the system operators can quickly initiate the frequency regulation process when either the SE, RE AC power systems, or the HVDC link suffers from a contingency that fluctuates the system frequency. To describe the whole contingency management process, a schematic diagram is illustrated in Fig. 8. In the case of HVDC link component failures, the normal converters conduct temporarily overloaded power transmission to mitigate the power imbalances, then the reserves of SE and RE AC power systems are dispatched to eliminate the abnormal frequency in their respective systems. Under generator failures, the frequency deviation signal at the fault end is converted to the opposite end through the HVDC link, and then fed into its frequency regulation flow to dispatch reserves. The whole process does not end until the frequency deviation eliminates.

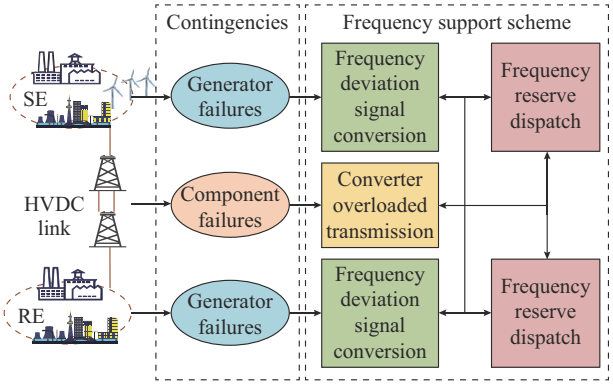

Fig. 8. Schematic diagram of contingency management process.

V. Reliability Indices and Evaluation Procedure

A. Formulation of System Reliability Indices

To evaluate the impact of the HVDC link and the proposed frequency regulation scheme on the reliability performance of the interconnected power system in terms of frequency and energy, four reliability indices are given as follows.

1) Expected Abnormal Frequency Duration (EAFD)

EAFD is used to evaluate the expected duration of abnormal system frequency, which can be represented by the shaded areas in Fig. 7. EAFD is calculated as:

$$EAFD = \sum_{t}\sum_{s\in S} p_{t,s}\left(TS_s^A + TR_s^A\right) \tag{19}$$

2) Expected Number of Frequency Insecurity (ENFI)

The rate-of-change-of-frequency (RoCoF) and the frequency nadir are the two typical metrics adopted to evaluate the system frequency security [2]. RoCoF is the slope of the frequency right after system contingencies. According to the PFR model given in Fig. 5, RoCoF can be calculated by:

$$RoCoF = \left.\frac{\mathrm{d}\Delta f}{\mathrm{d}t}\right|_{t=0} = \frac{\Delta P}{2H} \tag{20}$$

Typically, when the RoCoF surpasses its limit shown in Fig. 7 or the frequency nadir f_N exceeds the under- and over-frequency limits shown in Fig. 7 during system contingencies, it is considered that the frequency instability event occurs [29]. ENFI is then used to evaluate the likelihood of such frequency instability events, which is the sum of the probabilities of the contingencies in which the frequency instability incident occurs:

$$ENFI = \sum_{t}\sum_{s\in S} p_{t,s}\left(IS_S + IS_R\right) \tag{21}$$

The security indicator (IS) including IS_S and IS_R can be obtained by:

$$IS = \begin{cases} 1 & |RoCoF| > R^L \text{ or } \left|f_N\right| > f^L \\ 0 & \text{otherwise} \end{cases} \tag{22}$$

3) Accumulated Frequency Deviation Expectation (AFDE)

During system contingencies, the PFR and SFR models are adopted to recover the frequency stability. However, the system frequency cannot be restored to the nominal value given in Fig. 7 immediately, and will be deviated from the nominal frequency for a while. To evaluate the extent of the frequency deviation during the whole frequency regulation process, AFDE is formulated as:

$$AFDE = \sum_{t}\sum_{s\in S} p_{t,s}\left(\int_0^{TS_s^P+TS_s^S}\left|\Delta f_{S,t}\right|\mathrm{d}t + \int_0^{TR_s^P+TR_s^S}\left|\Delta f_{R,t}\right|\mathrm{d}t\right) \tag{23}$$

These durations are illustrated in Fig. 7 and can be calculated by the iteration process introduced in [17].

4) Expected Energy Curtailment (EEC)

The regulation ability of the frequency response model is limited by the reserve capacity. In some system contingencies that cause under-frequency events in the RE AC power system, the frequency may not be restored to nominal value due to the shortage of reserve capacity. Under such a circumstance, load shedding is inevitable. EEC is used to evaluate the total energy losses caused by load shedding, which is defined as:

$$EEC = \sum_{t}\sum_{s\in S} p_{t,s}\cdot LSR_s \tag{24}$$

$$LSR_s = \int_0^T LSR_t\mathrm{d}t \tag{25}$$

B. Reliability Evaluation Procedure

The proposed system frequency indices can be evaluated by the MCS technique [19], which contains the following steps.

Step 1: for the current sample n, generate the state sequences of the HVDC link utilizing its multi-state model described in Section II and the state sequences of the generating units based on their two-state model described in Section III. Then, the system contingency is formulated.

Step 2: perform the frequency regulation scheme developed in Section IV to obtain the regulated frequency dynamics of both SE and RE AC power systems, which is similar to that shown in Fig. 7.

Step 3: update the value of reliability indices EAFD, ENFI, AFDE and EEC based on (19)-(25).

Step 4: determine the MCS stopping criteria $n \le N$. Update $n = n+1$ and go to *Steps 1-3* to calculate the reliability indices again until $n \le N$ is not satisfied. Otherwise, output the final EAFD, ENFI, AFDE, and EEC indices.

VI. Case Studies

In this section, a modified two-area reliability test system (RTS) is used to illustrate the proposed reliability model [30]. The SE and RE AC power systems are interconnected by an HVDC link, whose reliability parameters are obtained from [9], [12]. The rated ALR of the HVDC link P_t^N is 700 MW. The nominal voltage is 1 p.u. and the allowed voltage variation is 0.8 p.u. to 1.2 p.u.. The multi-state model parameters of the HVDC link are shown in Table II, where occ is the abbreviation of occurrence.

TABLE II
Multi-state Model of HVDC Link

ALR (%)	Probability	Frequency (occ/year)
100	0.9870	10.7324
75	0.0096	10.3249
50	0.0034	0.5373
25	3.0215×10^{-5}	0.0353
0	1.2587×10^{-6}	3.4739×10^{-4}

The control parameters of the frequency response models in SE and RE AC power systems are derived from [21], [22], illustrated in Table III.

TABLE III
Control Parameters of Frequency Response Models in SE and RE AC Power Systems

Parameter	Value	Parameter	Value
R	20	F_{HP}	0.3
H	2864.35	D	2.5
T_G	0.2	K_{AGC}	0.5
T_{CH}	0.3	T_{RH}	7
r_{k1}	15%	r_{k2}	20%

The nominal frequency is 50 Hz, the RoCoF limit is 0.6 Hz/s, and the over- and under-frequency limits are 50.5 and 49.5 Hz, respectively. The primary and secondary reserve capacities are both set to be 10%. r_v and r_f are 0.8 and 0.7 Hz/V, respectively. The sampling number N for MCS technique is set to be 300000. The units are committed based on power rating in descending order. Besides, all the units are assumed to share the reserve proportionally based on power rating, and the time period is one hour. The following case study is simulated though MATLAB 2016b combined with Simulink toolbox.

A. Effect of Frequency Support Provided by HVDC Link

In this case, based on the evaluation procedure depicted in Section V-B, the reliability assessment results of the interconnected power system with an HVDC link with different frequency support schemes are given in Table IV.

Through comparing the reliability indices with different frequency regulation schemes, it can be observed that by utilizing the local frequency reserve sources, the conventional frequency regulation scheme can enhance the reliability performance for both SE and RE AC power systems. Meanwhile, since the proposed frequency regulation scheme allows the frequency reserve sources to be mutually available through the HVDC link, it reduces the value of the reliability indices further and improves the system reliability performance more significantly.

TABLE IV
Reliability Assessment Results of Interconnected Power System with an HVDC Link with Different Frequency Support Schemes

Scheme	Area	EAFD (hour/year)	ENFI (occ/year)	AFDE (Hz/year)	EEC (MWh/year)
No scheme	RE	0.15	262.5	1603.7	918.9
	SE	0.24	262.5	2121.3	510.0
	Total	0.39	525.0	3725.0	1428.9
Conventional scheme	RE	0.15	262.5	1367.9	732.6
	SE	0.06	262.5	1459.1	362.8
	Total	0.21	525.0	2827.0	1095.4
Proposed scheme	RE	0.11	179.3	943.2	598.5
	SE	0.06	179.3	1128.7	275.5
	Total	0.17	358.6	2071.9	874.0

B. Effect of Frequency Reserve Capacity

This case analyzes the effect of frequency response reserve capacity on system reliability. Both the primary and secondary reserve capacities increase from 5% to 15%. The results are shown in Fig. 9. It is clear from the numerical results that ENFI keeps invariable while the other three reliability indices are reduced significantly with the increase of the primary and secondary reserve capacities. The constant ENFI in Fig. 9(b) indicates that the increasing reserve does not affect the initial sharp change interval of abnormal frequency. The reason may be that the reserve capacity is not fully adopted in this interval. Besides, when both the primary and secondary reserve capacities exceed 13%, the change of AFDE, EAFD, and EEC becomes insignificant. The reason may be that when these reserves reach their critical capacity values, the marginal utility of reserve increment for improving frequency reliability is decreasing. Furthermore, with the increase of primary reserve, both EAFD and AFDE in Fig. 9(a) and (c) fall more significantly compared with the ones with the increase of the secondary reserve. However, the decrease of EEC in Fig. 9(d) is the opposite of EAFD and AFDE. A preliminary conclusion can be drawn that the duration and deviation of abnormal frequency are more affected by the primary reserve variance, while the energy losses are more subject to the secondary reserve variance.

C. Effect of HVDC Penetration Levels

In this case, the effect of the different HVDC penetration levels on system reliability is analyzed. Here, the HVDC penetration level refers to the ratio between the installed transmission capacity of the HVDC link and the installed generation capacity of the RE AC power system. Through adding the installed HVDC link transmission capacity, the HVDC penetration level increases from 20% to 40%. The effects of HVDC penetration levels on reliability indices are given in Fig. 10. It is clear that a rising tendency of the four

indices is illustrated with the increase of HVDC penetration levels. This may be because the increase of HVDC penetration level reduces the system inertia and lifts the occurrence probability of bulk power imbalance caused by HVDC link outages. As mentioned in the introduction, the HVDC link connects asynchronous AC power systems through the non-synchronous interfaces. When the HVDC penetration level increases, the power flowing through the non-synchronous interfaces through the HVDC link lifts, which, therefore, cuts down the system inertia. Besides, the increase of power flow from the HVDC link will reduce the power output from synchronous generators in RE AC power system, which can also reduce the system inertia since these synchronous generators are the main source of inertia.

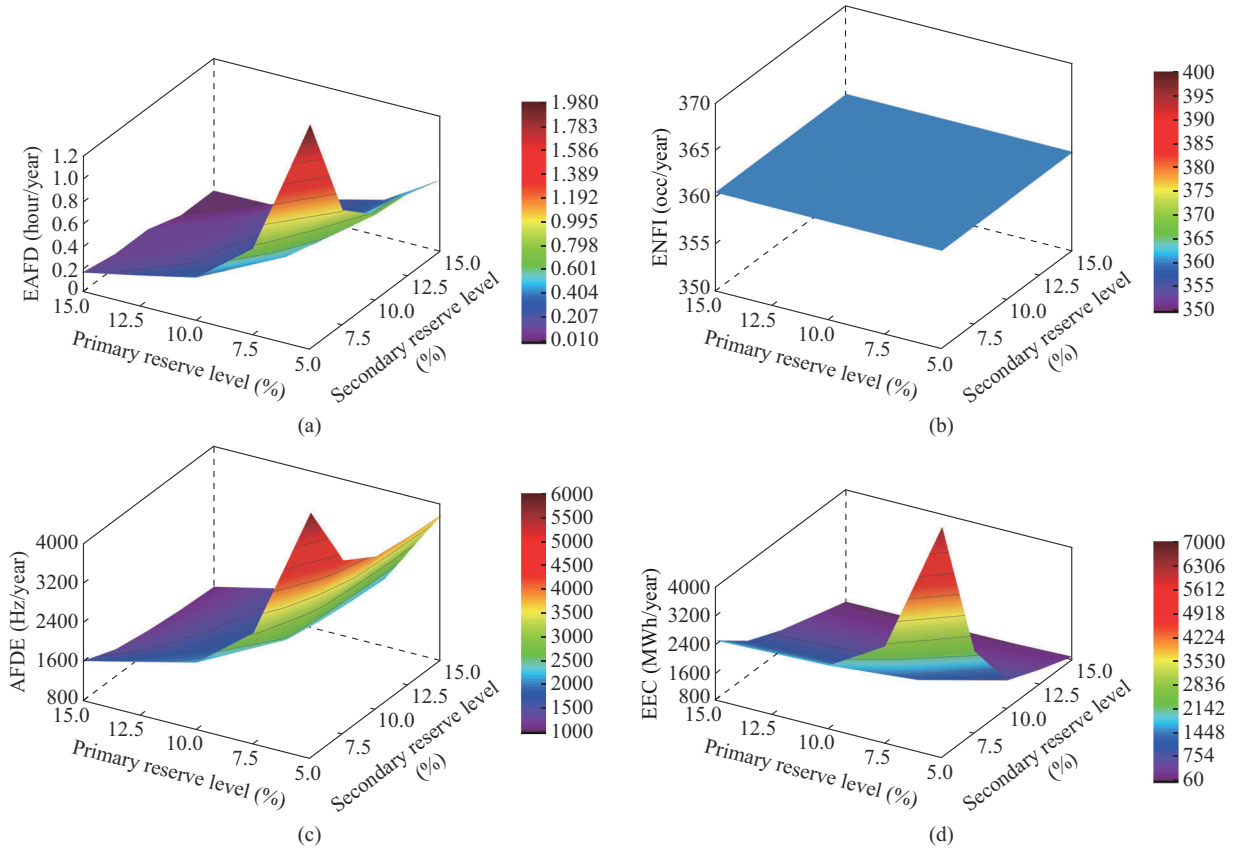

Fig. 9. Effect of reserve capacities on reliability indices. (a) EAFD. (b) ENFI. (c) AFDE. (d) EEC.

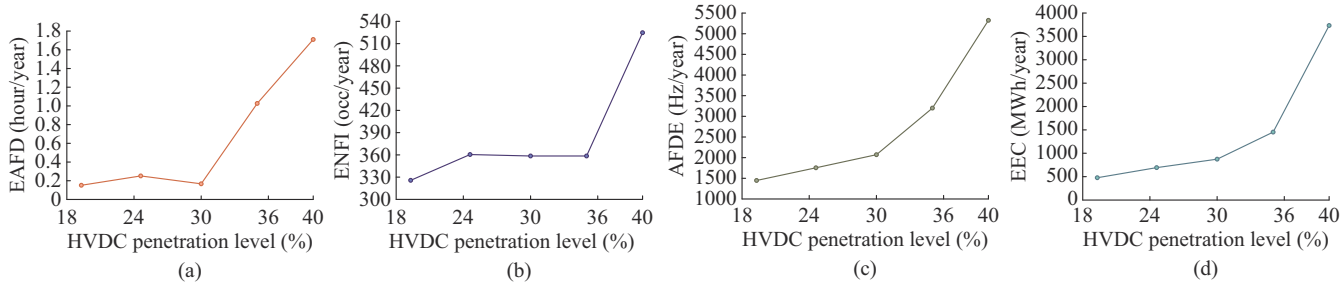

Fig. 10. Effects of HVDC penetration levels on reliability indices. (a) EAFD. (b) ENFI. (c) AFDE. (d) EEC.

Meanwhile, all the four indices present a sharp rise when the HVDC penetration level is higher than a specific value; while in other intervals, they change quite slowly. For instance, ENFI changes smoothly when the HVDC penetration level is lower than 35% while lifting sharply after the HVDC penetration level exceeds 35%. Such a profile may stem from the fact that when the HVDC penetration level exceeds a critical high value, the existing reserve of the RE AC power system cannot cover the power imbalance caused by the HVDC link outages. Therefore, both the energy losses and frequency deviation of the RE AC power system have a significant increase. Besides, the reduced system inertia also makes the abnormal frequency duration become longer. It can be concluded that the HVDC penetration level should match the existing reserve level to keep a good reliability performance of the whole power system.

VII. Conclusion

This paper develops a multi-state model of an HVDC link by investigating its different ALRs and the corresponding probabilities subject to component outages. A framework to

evaluate the reliability of the interconnected power system is established with a novel frequency regulation scheme provided by the HVDC link.

The effects of different HVDC penetration levels and reserve capacities on the system reliability performance in terms of frequency dynamics during its regulation process are analyzed. Simulation results obtained from a modified two-area RTS indicate that the frequency regulation scheme provided by the normal converters of the HVDC link can improve the reliability performance of the interconnected power system. Specifically, it can effectively decrease the abnormal frequency duration, reduce the frequency deviation, and cut down the energy loss compared with the conventional frequency regulation scheme, which should therefore be adopted for frequency regulation during the system contingencies. Besides, it is also found from the simulation results that different kinds of the reserve can lift the frequency reliability of the interconnected system in different aspects. In detail, the primary reserve can better help reduce the duration and deviation of abnormal frequency, while the secondary reserve can better relieve the energy loss during system contingencies. Furthermore, the increase of HVDC penetration level may significantly deteriorate the system reliability if the existing reserve is unable to cover the power imbalance caused by the HVDC link outage. Therefore, more reserve is needed when the transmission capacity of the HVDC link increases.

The above results provide a reference to evaluate the risks of interconnected power systems with the ever-spreading HVDC projects in terms of frequency security at the system planning stage. Besides, the proposed technique can guide the system operators to comprehensively dispatch the reserves in the interconnected power system according to their frequency reliability preference by fully utilizing the overload transmission capability of the HVDC link.

REFERENCES

[1] T. J. Hammons, V. F. Lescale, K. Uecker *et al*., "State of the art in ultrahigh-voltage transmission," *Proceedings of the IEEE*, vol. 100, no. 2, pp. 360-390, Feb. 2012,

[2] Y. Wen, C. Y. Chung, and X. Ye, "Enhancing frequency stability of asynchronous grids interconnected with HVDC links," *IEEE Transactions on Power Systems*, vol. 33, no. 2, pp. 1800-1810, Mar. 2018.

[3] X. Qin, P. Zeng, Q. Zhou *et al*., "Study on the development and reliability of HVDC transmission systems in China," in *Proceedings of 2016 IEEE International Conference on Power System Technology (POWERCON)*, Wollongong, Australia, Nov. 2016, pp. 1-6.

[4] M. Waseem, Z. Lin, Y. Ding *et al*., "Technologies and practical implementations of air-conditioner based demand response," *Journal of Modern Power Systems and Clean Energy*, vol. 9, no. 6, pp. 1395-1413, Nov. 2021.

[5] C. Chen, K. Zhang, M. Ni *et al*., "Cyber-attack-tolerant frequency control of power systems," *Journal of Modern Power Systems and Clean Energy*, vol. 9, no. 2, pp. 307-315, Mar. 2021.

[6] J. O'Sullivan, A. Rogers, D. Flynn *et al*., "Studying the maximum instantaneous non-synchronous generation in an island system–frequency stability challenges in Ireland," *IEEE Transactions on Power Systems*, vol. 29, no. 6, pp. 2943-2951, Nov. 2014.

[7] X. Wu, Q. Lan, Z. Li *et al*., "Frequency characteristics of East China power grid after bipolar locking of ultra-high voltage direct current (UHVDC)," *The Journal of Engineering*, vol. 2017, no. 13, pp. 1237-1241, Jan. 2017.

[8] B. Wang, X. Wang, Z. Bie *et al*., "Reliability model of MMC considering periodic preventive maintenance," *IEEE Transactions on Power Delivery*, vol. 32, no. 3, pp. 1535-1544, Jun. 2017

[9] Y. Ma, S. Li, Y. Hua *et al*., "Reliability evaluation to converter transformers of 2×12-pulse UHVDC transmission system," in *Proceedings of 2014 China International Conference on Electricity Distribution (CICED)*, Shenzhen, China, Sept. 2014, pp. 219-222.

[10] B. Hu, K. Xie, and H. Tai, "Reliability evaluation and weak component identification of ±500 kV HVDC transmission systems with double-circuit lines on the same tower," *IEEE Transactions on Power Delivery*, vol. 33, no. 4, pp. 1716-1726, Aug. 2018.

[11] S. Li, Y. Ma, Y. Hua *et al*., "Reliability equivalence and sensitivity analysis to UHVDC systems based on the matrix description of the F&D method," *IEEE Transactions on Power Delivery*, vol. 31, no. 2, pp. 456-464, Apr. 2016.

[12] X. Jiang, C. Ye, Y. Ding *et al.*, "Reliability equivalence to symmetrical UHVDC transmission systems considering redundant structure configuration," *Energies*, vol. 11, no. 4, pp. 753, Apr. 2018.

[13] D. Wu, N. Zhang, C. Kang *et al.*, "Techno-economic analysis of contingency reserve allocation scheme for combined UHV DC and AC receiving-end power system," *CSEE Journal of Power Energy System*, vol. 2, no. 2, pp. 62-70, Jun. 2016.

[14] E. Rakhshani, H. Mehrjerdi, N. A. Al-Emadi *et al.*, "On sizing the required energy of HVDC based inertia emulation for frequency control," in *Proceedings of 2017 IEEE PES General Meeting*, Chicago, USA, Jul. 2017, pp. 1-5.

[15] Y. Song, J. Zhang, Y. Zhao *et al*., "Sending end frequency and voltage under islanded operation mode of HVDC transmission system," in *Proceedings of 2017 IEEE Conference on Energy Internet and Energy System Integration (EI2)*, Beijing, China, Nov. 2017, pp. 1-6.

[16] B. Silva, C. L. Moreira, L. Seca *et al*., "Provision of inertial and primary frequency control services using offshore multiterminal HVDC networks," *IEEE Transactions on Sustainable Energy*, vol. 3, no. 4, pp. 800-808, Oct. 2012.

[17] C. Liang, P. Wang, X. Han *et al*., "Operational reliability and economics of power systems with considering frequency control processes," *IEEE Transactions on Power Systems*, vol. 32, no. 4, pp. 2570-2580, Jul. 2017.

[18] A. Lisnianski, I. Frenkel, and Y. Ding, *Multi-state System Reliability Analysis and Optimization for Engineers and Industrial Managers.* London: Springer Science & Business Media, 2010.

[19] R. Billinton and R. N. Allan, *Reliability Evaluation of Engineering Systems*. New York: Plenum Press, 1992.

[20] K. Xie, B. Hu, and C. Singh, "Reliability evaluation of double 12-pulse ultra HVDC transmission systems," *IEEE Transactions on Power Delivery*, vol. 31, no. 1, pp. 210-218, Feb. 2016.

[21] P. Kundur, *Power System Stability and Control*. Palo Alto: EPRI, 1994.

[22] L. Guo, Y. Ding, M. Bao *et al*., "Nodal reliability evaluation for a VSC-MTDC-based hybrid AC/DC power system," *IEEE Transactions on Power Systems*, vol. 35, no. 3, pp. 2300-2312, May 2020.

[23] T. Shekari, F. Aminifar, and M. Sanaye-Pasand, "An analytical adaptive load shedding scheme against severe combinational disturbances," *IEEE Transactions on Power Systems*, vol. 31, no. 5, pp. 4135-4143, Sept. 2016.

[24] H. Chvez, R. Baldick, and J. Matevosyan, "The joint adequacy of AGC and primary frequency response in single balancing authority systems," *IEEE Transactions on Sustainable Energy*, vol. 6, no. 3, pp. 959-966, Jul. 2015.

[25] I. M. Sanz, P. D. Judge, C. E. Spallarossa *et al*., "Dynamic overload capability of VSC-HVDC interconnections for frequency support," *IEEE Transactions on Energy Conversion.* vol. 32, no. 4, pp. 1544-1553, Dec. 2017.

[26] P. D. Judge and T. C. Green, "Dynamic thermal rating of a modular multilevel converter HVDC link with overload capacity," in *Proceedings of 2015 IEEE Eindhoven PowerTech*, Eindhoven, Netherlands, Jul. 2015, pp. 1-6.

[27] M. K. Metwaly and J. Teh, "Fuzzy dynamic thermal rating system-based SIPS for enhancing transmission line security," *IEEE Access*, vol. 9, pp. 83628-83641, Jun. 2021.

[28] J. Teh, C.-M. Lai, N. A. Muhamad *et al.*, "Prospects of using the dynamic thermal rating system for reliable electrical networks: a review," *IEEE Access*, vol. 6, pp. 26765-26778, Apr. 2018.

[29] L. Sigrist, "A UFLS scheme for small isolated power systems using rate-of-change of frequency," *IEEE Transactions on Power Systems*, vol. 30, no. 4, pp. 2192-2193, Jul. 2015.

[30] P. M. Subcommittee, "IEEE reliability test system," *IEEE Transactions on Power Apparatus and Systems*, vol. PAS-98, no. 6, pp. 2047-2054, Nov. 1979.

Chengjin Ye received the B.E. and Ph.D. degrees from Zhejiang University, Hangzhou, China, both in electrical engineering, in 2010 and 2015, respectively. He served as a Distribution System Engineer for the Economics Institute of State Grid Zhejiang Electric Power Co., Ltd., Hangzhou, China, from 2015 to 2017. He was a Postdoc Researcher in Zhejiang University from 2017 to 2019. From 2020, He serves as a Research Professor with the College of Electrical Engineering, Zhejiang University. His research interests include planning and operation of data-driven power system, short-circuit current limitation, and integration of demand-side resources into power system.

Libang Guo received the B.S. degree in electrical engineering from Huazhong University of Science and Technology, Wuhan, China. He is currently pursuing the Ph. D. degree in electric engineering in Zhejiang University, Hangzhou, China. His research interests include reliability analysis and protection of hybrid AC/DC power system and electricity market.

Yi Ding received the bachelor's and Ph.D. degrees in electrical engineering from Shanghai Jiao Tong University, Shanghai, China, and Nanyang Technological University, Singapore, in 2002 and 2007, respectively. He is a Professor with the College of Electrical Engineering, Zhejiang University, Hangzhou, China. His current research interests include reliability analysis of power system integrated with renewable energy resources, smart grid performance analysis, and reliability modeling and optimization of engineering systems.

Ming Ding received the B.Sc. and M.Sc. degrees from Hefei University of Technology, Hefei, China, and Xi'an Jiaotong University, Xi'an, China, in 1981 and 1984, respectively. He is now a Professor of Electrical Engineering and Automation, Hefei University of Technology, a Senior Member of Chinese Society for Electrical Engineering (CSEE), Member of Reliability Committee of CSEE, and Member of Reliability Management Committee of State Electricity Regulatory Commission. His research interests include reliability and security of power system, renewable energy and distributed generation system, and application of power electronics in power systems.

Peng Wang received the Ph. D. degree from the University of Saskatchewan, Saskatoon, Canada. He is currently a Professor with the Electrical and Electronic Engineering School, Nanyang Technological University, Singapore. His research interests include planning and operation of power system, renewable energy planning, solar/electricity conversion systems, electricity market, and reliability analysis of power system.

Lei Wang received the M.S. degree from Tsinghua University, Beijing, China. She is an Engineer at the Center of Planning and Assessment, State Grid Zhejiang Economic Research Institute, Hangzhou, China. Her research interests include planning and operation of power system.